

# Influence of the photoionization cross-section on the OSL signal of LiF: A theoretical and experimental approach

Bruna Novais<sup>a</sup>, Edward Ferraz<sup>b</sup>, Adelmo S. Souza<sup>c</sup>, Patrícia L. Antonio<sup>d</sup>, Linda V.E. Caldas<sup>d</sup>, João Batista<sup>e</sup>, Heveson Lima<sup>a,\*</sup>

<sup>a</sup> Multidisciplinary Center of Luís Eduardo Magalhães, Federal University of Western Bahia, 47850-000 Luís Eduardo Magalhães, BA, Brazil

<sup>b</sup> Center for Exact Sciences and Technologies, Federal University of Western Bahia, 47808-021 Barreiras, BA, Brazil

<sup>c</sup> Multidisciplinary Center of Bom Jesus da Lapa, Federal University of Western Bahia, 47600-000 Bom Jesus da Lapa, BA, Brazil

<sup>d</sup> Institute of Energy and Nuclear Research, Brazilian Nuclear Energy Commission, 05508-000 São Paulo, SP, Brazil

<sup>e</sup> Federal University of Health Sciences of Porto Alegre, 91310-002 Porto Alegre, RS, Brazil

## ARTICLE INFO

### Keywords:

Photoionization cross-section  
Personal dosimeter  
Optically stimulated luminescence  
Lithium fluoride

## ABSTRACT

The understanding of the electron trapping and recombination processes is the key to successful applications of materials in ionizing radiation dosimetry, which unfortunately are not well known yet. In this work, the influence of the photoionization cross-section ( $\sigma$ ) was investigated on the optically stimulated luminescence (OSL) response of the lithium fluoride (LiF) compound. The  $\sigma$  has been predicted through the expression proposed by Lima–Batista–Couto. In addition, OSL measurements were performed using the continuous-wave stimulation mode (CW-OSL), with 60 s of light stimulation. The samples were submitted to 10 Gy and 15 Gy of absorbed dose. Phonon dispersion and density calculations are presented by using the Density Functional Perturbation Theory. The results, obtained by a combination of different methodologies, show that the low sensitivity of LiF to the light stimulus ( $\lambda = 470$  nm) is due to the very low magnitude of  $\sigma$  at the used excitation wavelength. A comparison with  $\text{Al}_2\text{O}_3\text{:C}$  was also carried out, showing that the intensity and the pattern of the OSL curve decay are modified by the  $\sigma$ . These results play an important role in understanding the luminescent properties of this material, and they open a new opportunity to improve the light sensitivity of this detector.

## 1. Introduction

The use of ionizing radiation is a fact in many different applications as medical procedures (for both diagnostic and therapeutic purposes) [1,2] and industry [3], for instance. Considering this fact, ionizing radiation dosimetry has been an active research field for many years. A common technique to estimate the absorbed radiation dose involves the use of luminescent properties of specific insulators and semiconductors. Two main exponents of the luminescence-based techniques for radiation dosimetry are the optically stimulated luminescence (OSL) [4] and the thermoluminescence (TL) [5,6]. Some advantages of OSL over TL [7] have called attention to the application of this technique in ionizing radiation dosimetry field in the last decades. Among many researched materials that fit the requisites to be used as TL dosimeters, Lithium Fluoride (LiF) doped with different elements has received attention along the years (LiF:Mg,Ti - TLD 100; LiF:Mg,Cu,P; etc.) [8,9]. However, TL is a destructive technique, and it is not suitable for high spatial resolution imaging. Regarding OSL dosimeters, Carbon-doped Aluminum Oxide ( $\text{Al}_2\text{O}_3\text{:C}$ ) can be considered as one of the most used and studied.

Even though the theoretical background of the two quoted techniques can be considered as similar to each other, the differences in the stimulation process (optical for OSL, thermal for TL) implicate in different approaches both experimentally and in theoretical studies.

Lithium Fluoride is an insulator that crystallizes in fcc structure with a band gap around 14 eV [10]. The interest in using LiF as a matrix for TL dosimeters is based on characteristics as the effective atomic number similar to the human tissue (7.7 [11]), potential use for neutron detection (using Li-6), low fading, high levels of stimulated luminescence signal when doped, etc. Considering the search for new OSL dosimeters [12,13], several works have performed doping and co-doping processes using different elements to study the dosimetric behavior of LiF with optical stimulus [14–16]. Comprehending the physical processes that underlie the OSL emission of different materials is an important and essential approach towards the evolution in designing new dosimeters for different applications [17]. To the best of our knowledge, a specific theoretical analysis and explanation to the low OSL emission from the undoped LiF has not been presented yet.

\* Corresponding author.

E-mail address: [heveson.matos@ufob.edu.br](mailto:heveson.matos@ufob.edu.br) (H. Lima).

<https://doi.org/10.1016/j.optmat.2020.109792>

Received 6 December 2019; Received in revised form 10 February 2020; Accepted 20 February 2020

Available online 3 March 2020

0925-3467/© 2020 Elsevier B.V. All rights reserved.

Several models have been used to describe the stimulated luminescence behavior of physical systems, for instance: one-trap/one-recombination-center model (OTOR) and multiple trap levels and recombination centers [18]. In all cases, the OSL intensity is proportional to the photoionization cross-section ( $\sigma$ ) and other rate parameters. Predicting the values of those parameters, as well as providing a relation with the experimental data, there still remains a challenge in some points. The arbitrary units in the experimental measures (which make impossible a direct relation with the rate parameters) and the fact that the number of parameters is greater than the number of rate equations that describe the OSL mechanism (making impossible an exact solution) are examples of why this challenge remains. For the  $\sigma$  prediction, this situation can be overcome by using the expression proposed by Lima–Batista–Couto [19].

The photoionization cross-section is of fundamental importance to understand the optical properties of insulators and semiconductors. It has been used widely to characterize defects and impurities in crystalline materials [20,21], spherical quantum dots [22] and to interpret hard X-ray photoemission spectroscopic spectra of NiO [23].

The aim of this work was to analyze the influence of the photoionization cross-section on the OSL signal of LiF, using the expression proposed by Lima–Batista–Couto. In addition, experimental results of the OSL signal intensity versus time of stimulation are presented, and a comparison between the signals obtained with LiF and  $\text{Al}_2\text{O}_3\text{:C}$  is provided. Phonon dispersion and density calculations are also presented by using the Density Functional Perturbation Theory, and the influence of the phonon frequency on the OSL signal is discussed.

## 2. Experimental procedure

Samples of lithium fluoride (LiF — prepared from the undoped LiF powder produced by Merck, product number: 232-152-0, 25.94 molar mass, as pellets with 6 mm diameter and 0.8 mm thickness) and carbon-doped aluminum oxide ( $\text{Al}_2\text{O}_3\text{:C}$  - TLD-500, produced by Rexon, as pellets with 5 mm diameter and 1.0 mm thickness) were used in order to compare their optically stimulated luminescence signals.

OSL measurements were performed in a TL/OSL Risø Reader using the continuous wave stimulation mode (CW-OSL), performed with 60 s of light stimulation. A beta radiation source of  $^{90}\text{Sr}+^{90}\text{Y}$  (dose-rate of  $\sim 81.6$  mGy/s at the sample position) coupled to the reader was used in all irradiation procedures. Blue LEDs (emission peak at 470 nm,  $\sim 72$  mW/cm<sup>2</sup>) and a filter Hoya U-340 (transmission between 290 nm and 390 nm) were used as stimulation light and to discriminate OSL emission and stimulation wavelength, respectively. The samples of LiF were submitted to 10 Gy and 15 Gy of absorbed dose. The samples of  $\text{Al}_2\text{O}_3\text{:C}$  were submitted to 170 mGy of absorbed dose. Relatively high doses of radiation had to be used in case of the undoped samples in view of getting a clear signal from those samples using the above mentioned settings. The time spent between irradiation and OSL measurement was 0 s; all measurements were taken immediately after irradiation. This time was adopted as a standard, and it was used for all the samples of both materials (LiF and  $\text{Al}_2\text{O}_3\text{:C}$ ), in order to avoid any unwanted influence on obtaining the OSL signal. No collimator was used in the measurements.

OSL reproducibility assessments were performed for groups of at least 3 pellets from each composition. Emitted signals are presented as the average of the utilized samples. In view of comparing the patterns of OSL signal decay, normalized curves were plotted for each composition.

## 3. Theory

### 3.1. Single trap level model

Optically stimulated luminescence is a transient luminescence observed during the light stimulus (generally in the blue region) of

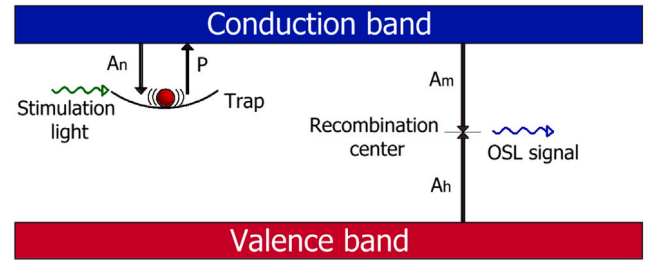


Fig. 1. Representation of an OSL simple model with one trap and one recombination center.  $P$ ,  $A_n$ ,  $A_m$  and  $A_h$  are the rate parameters of the transition.

insulators and semiconductors that were previously exposed to ionizing radiation.

In the simplest model of the OSL process only two levels are used in the band gap of the material as shown in Fig. 1. One is the trap where the electrons are accumulated during the exposure to ionizing radiation, and the other is the hole trap that acts as a recombination center [4,24]. Assuming the first order kinetic approximation (no retrapping), the concentration of trapped electrons ( $n$ ) will change according to

$$\frac{dn}{dt} = -n\sigma\varphi \quad (1)$$

where  $\sigma$  is the photoionization cross-section ( $m^2$ ) and  $\varphi$  is the stimulated photon flux with wavelength  $\lambda$  ( $m^{-2}s^{-1}$ ). Note that  $p=\sigma\varphi$  represents the detrapping probability rate.

Solving Eq. (1) it is easy to show that  $n$  decays exponentially with the stimulation time. Thus,

$$n(t) = n_0 e^{-\sigma\varphi t} \quad (2)$$

where  $n_0$  is the initial concentration of trapped electrons at  $t=0$ . The intensity of the emitted light is proportional to the rate of electrons escaping from the trapping level,  $dn/dt$ . So, if combining Equations (1) and (2):

$$I_{OSL}(t) \propto \left| \frac{dn}{dt} \right| = n_0 \sigma \varphi e^{-\sigma\varphi t} \quad (3)$$

The OSL intensity decays exponentially during the light stimulus. Eq. (3) shows a dependence between  $I(t)$  and  $\sigma$ . For some materials (e.g.  $\text{Al}_2\text{O}_3\text{:C}$ , LiF:Mg,Ti and BeO) this behavior has already been observed [25,26]. In fact, it is possible to determine the sensitivity of the material through  $\sigma$ .

### 3.2. Photoionization cross-section

The photoionization cross-section is one of the most important physical quantities to understand the transition mechanisms in metastable levels containing the media. Recently, Lima–Batista–Couto [19] have proposed a model to calculate the  $\sigma$  based on the time-dependent perturbation theory. This expression is obtained considering that the radiation field which interacts with the trapped electrons is semiclassical and linearly polarized. Thus, the probability of the electron to be promoted to the conduction band is described by the  $\sigma$  which is a function of the photon energy and is given by Eq. (4) [27]

$$\sigma = \frac{4\pi^2 \hbar}{m^* \omega} \left( \frac{e^2}{\hbar c} \right) |\langle n | e^{i(\omega/c)(\hat{n}\cdot\mathbf{x})} \hat{\mathbf{e}} \cdot \mathbf{p} | \psi_0 \rangle|^2 \rho(E_n) |_{E_n \cong E_i - \hbar\omega} \quad (4)$$

where  $\omega$  is the angular frequency of the incident electromagnetic radiation,  $E_i$  is the activation energy of the donor impurity level,  $E_n$  is the energy of the final state,  $m^*$  is the electron effective mass,  $\mathbf{p}$  is the electron linear momentum vector,  $\hat{\mathbf{e}}$  and  $\hat{\mathbf{n}}$  are the polarization and propagation directions, respectively.  $|\psi_0\rangle$  and  $|n\rangle$  are wave functions of the trap state

and the continuum final state, respectively.  $\langle n|e^{i(\omega/c)(\hat{n}\cdot\mathbf{x})}\hat{\mathbf{e}}\cdot\mathbf{p}|\psi_0\rangle$  is the transition matrix element and  $\rho(E_n)$  is the final density of states.

As the electron moves almost freely in the conduction band,  $|n\rangle$  can be described approximately as a plane wave in the continuum final state. The plane wave function used in another theoretical methodology [22] for calculating  $\sigma$  is given by

$$|n\rangle = \frac{1}{\sqrt{L^3}} e^{i\mathbf{k}\cdot\mathbf{x}} \quad (5)$$

where  $L^3$  is the volume of the system, and  $\mathbf{k}$  is the wave vector of the electron. From the energy conservation, one has

$$k^2 = \frac{2m^*}{\hbar^2} (\hbar\omega - E_i) \quad (6)$$

The electron promoted to the conduction band, by the ionizing radiation, undergoes various collisions with other electrons. Instead of returning to the valence band, the electron is captured by impurity levels which are created by defects and vacancy in the material. Electron levels in the potential well may be considered like localized states, and the electron in this states oscillates locally with an angular frequency,  $\omega_0$ , which depends on the phonon vibrations of the crystal lattice. In this way, the donor impurity wave function can be described, approximately, as the ground state of a three-dimensional isotropic harmonic oscillator of angular frequency  $\omega_0$  (see Fig. 1). In the ground state, the electron remains in the lowest energy state, and the lifetime is infinite if there is not the action from external forces. Thus,  $|\psi_0\rangle$  is given by

$$|\psi_0\rangle = \left(\frac{m^*\omega_0}{\pi\hbar}\right)^{3/4} e^{-\frac{m^*\omega_0}{2\hbar}x^2} \quad (7)$$

where  $\mathbf{x}$  is three-dimensional vector in the Cartesian space.

The final density of states  $\rho(E_n)$  in the conduction band can be obtained by using a simple box normalization convention, of side  $L$ , for the plane wave states. Thus,  $\rho(E_n)$  within a solid angle  $d\Omega$  is given by

$$\rho(E_n) = \left(\frac{L}{2\pi}\right)^3 \frac{m^*}{\hbar^2} k d\Omega \quad (8)$$

By using the Fermi's golden rule and the wave functions (Eq. (5) and Eq. (7)) in Eq. (4):

$$\sigma = \frac{4\alpha\hbar^2 k^3}{m^{*2}\omega\omega_0} \sqrt{\frac{\pi\hbar}{m^*\omega_0}} \exp\left\{-\frac{\hbar}{m^*\omega_0} \left[k^2 + \left(\frac{\omega}{c}\right)^2\right]\right\} \times 4\pi \left(\frac{1}{\gamma(\omega)}\right)^3 [\gamma(\omega) \cosh(\gamma(\omega)) - \sinh(\gamma(\omega))] \quad (9)$$

where  $\gamma(\omega) = 2k\hbar\omega/m^*\omega_0 c$  is an energy function [19]. This model was obtained using all multipole terms in the Hamiltonian, without considering the approximation of electric dipole.

Eq. (9) describes the probability of the trapped electron to be promoted to the conduction band and, subsequently, to be recombined with a hole, in the luminescent center, through the stimulus of the electromagnetic radiation. Note that Eq. (9) takes into account the competition between the radiative and non-radiative transitions through the dependence with  $\omega$  and  $\omega_0$ . It is important to understand the sensibility of the trapped electrons to the light stimulus. Furthermore, there is a dependence with the electron effective mass which takes into account the mobility of the electrons in the host material.

### 3.3. Density functional theory

The framework adopted for the present calculations is the Density-Functional Theory (DFT), using a Plane-Wave basis set and pseudopotentials for the Fluorine and Lithium atoms, within its generalized gradient approximation (GGA) for exchange–correlation energy as improved by Perdew–Burke–Ernzerhof [28]. The calculation of phonons was carried out after the self-consistent calculation, using the Density-Functional Perturbation Theory as implemented in the

**Table 1**

Physical quantities used to predict  $\sigma$  and the reference from where it was taken from. me stands for the electron mass.

Quantity	LiF	Al <sub>2</sub> O <sub>3</sub> :C
E <sub>i</sub> (eV)	0.97 [32]	2.4 [33,34]
m* (me)	2.16 [35]	0.22 [36]
ω <sub>0</sub> (THz)	65.8 (This work)	1.63 [37]

Quantum Espresso code [29,30]. The Kinect-energy cutoff was 50.0 Ry, charge density cutoff 200.0 Ry. The system adopted for the simulations was the Lithium Fluoride, a cubic structure, space group F m  $\bar{3}$  m, containing two atoms in the unit cell, and a lattice constant of a = 4.0270 Å. Such size for the cell was adopted for fast calculation to phonon dispersion.

## 4. Results and discussion

The reproducibility of the batch of pellets used in the analysis was studied. At least three samples of each composition were submitted to five cycles or more of the irradiation-reading process. For each batch of samples, no more than 12% of variation regarding both the total emitted signal represented by the integral value below the OSL curve and the emission on the very first 0.24 s (minimum integration time in the value of the counts during obtaining the OSL signal, taking into account the maximum time of 60 s and the number of points equal to 250 (points of the OSL curve)) was verified.

As expected, Fig. 2a shows that even though the absorbed dose is greatly lower in the case of Al<sub>2</sub>O<sub>3</sub>:C, its OSL emission intensity is significantly higher than the one from LiF. Fig. 2b shows different patterns of decays represented with normalized curves, in which a faster decay pattern from Al<sub>2</sub>O<sub>3</sub>:C is seen than in LiF. Normalization was performed based on the highest value of emission during light stimulation.

Fig. 3a shows that the emitted OSL intensity from LiF is higher when the samples are submitted to 15 Gy than to 10 Gy. At the same time it is seen that regarding the pattern of decay, there is no such difference when the normalized OSL curves are analyzed (Fig. 3b).

Parameters as the initial concentration of trapped charge carriers ( $n_0$ ) in the trapping center, the wavelength-dependent photoionization cross-section  $\sigma(\lambda)$ , and the stimulation photon-flux reaching the detector  $\varphi(\lambda)$  are important in the considerations of the mechanisms behind the OSL signal characteristics. By using the theoretical approach of the photoionization cross-section of the trapping centers in both materials, LiF and Al<sub>2</sub>O<sub>3</sub>:C, it is possible to explain the OSL decay pattern as well as the reason why the intensity of the OSL emission signal of LiF is significantly lower than of Al<sub>2</sub>O<sub>3</sub>:C. This discussion will be based on the first-order kinetic model for OSL, which assumes the absence of retrapping process. In fact, this analysis is valid no matter the energy of the ionizing radiation, that was used in both materials, because the peak of maximum temperature on TL signal does not shift with the energy of the ionizing radiation in most of the dosimeter materials [31] as well as the OSL decay pattern remains the same for both doses (10 and 15 Gy for LiF).

The photoionization cross-section ( $\sigma$ ) of both materials was predicted through the model proposed by Lima–Batista–Couto [19], based on time-dependent perturbation theory, as described in section Theory. Eq. (5) depends on some physical quantities (such as activation energy, electron effective mass, phonon frequency) and one variable (the frequency of electromagnetic radiation used as stimulus). For Al<sub>2</sub>O<sub>3</sub>:C, a detailed discussion about  $\sigma$  was carried out in a previous work [19] by using three different activation energies and electron effective masses. The purpose of using it here is for comparison purposes with the LiF compound. Table 1 presents these physical quantities for both materials.

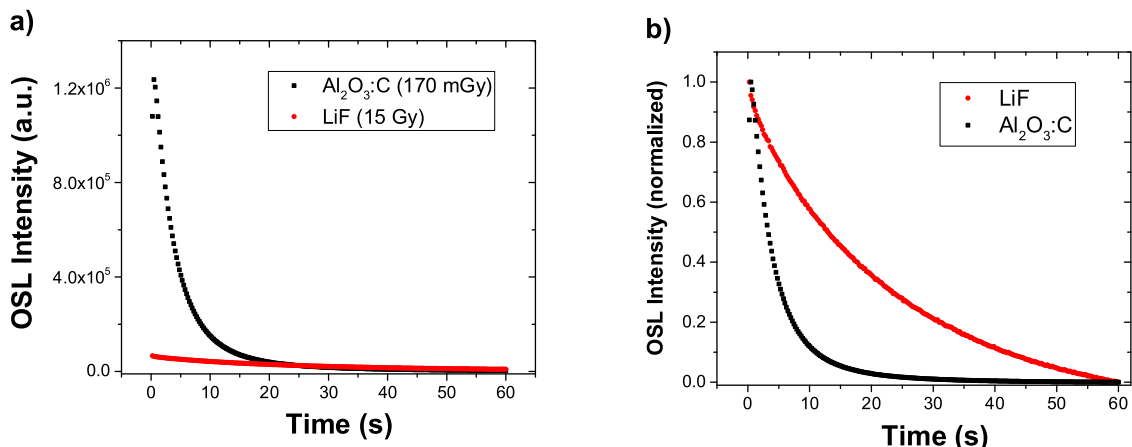


Fig. 2. (a) OSL emission curves for the  $\text{Al}_2\text{O}_3:\text{C}$  and LiF samples irradiated using different absorbed doses values; (b) Normalized OSL curves.

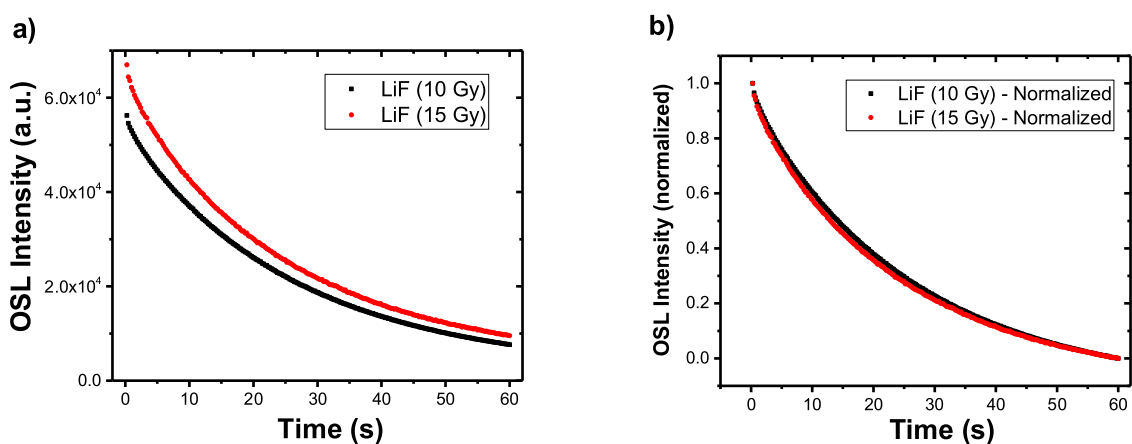


Fig. 3. (a) OSL emission from LiF irradiated with 10 Gy and 15 Gy; (b) Normalized curves.

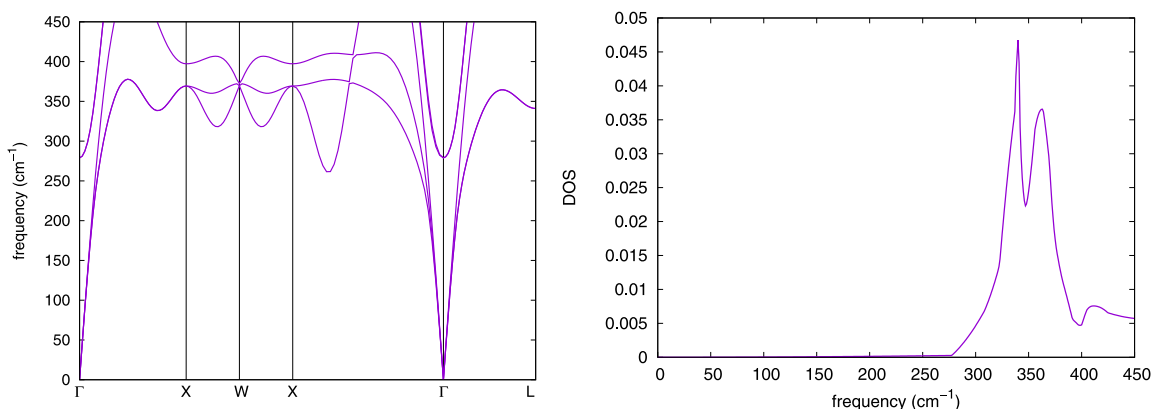


Fig. 4. (a) Phonon dispersion and (b) Phonon density of LiF compound.

In particular, for the LiF compound the phonon frequency has been obtained through the Density-Functional Perturbation Theory as implemented in the Quantum Espresso code. Fig. 4a and 4b show the phonon dispersion and phonon density, respectively. In the interval between  $300\text{ cm}^{-1}$  and  $350\text{ cm}^{-1}$ , there is a contribution peak of the lithium atom and in the interval between  $350\text{ cm}^{-1}$  and  $400\text{ cm}^{-1}$ , there is a greater contribution of the atom of fluorine. Note that the atom of fluorine has a major contribution to the non-radiative transitions in this compound. The phonon frequency (Table 1) obtained here shows

a close agreement to literature predictions [38], and it was used for calculating  $\sigma$ .

In order to analyze the behavior of Eq. (9), the photoionization cross section was plotted as a function of the electromagnetic radiation energy for both materials. Note that in Fig. 5 the probability distribution curve presents one maximum about 2.6 eV for the  $\text{Al}_2\text{O}_3:\text{C}$  (red line), and another about 1 eV for the LiF (blue line). These peaks correspond to the maximum probabilities of the electron in the trapping centers to be excited to the conduction band and, subsequently, to be recombined with a hole in a recombination center emitting a luminescent signal.

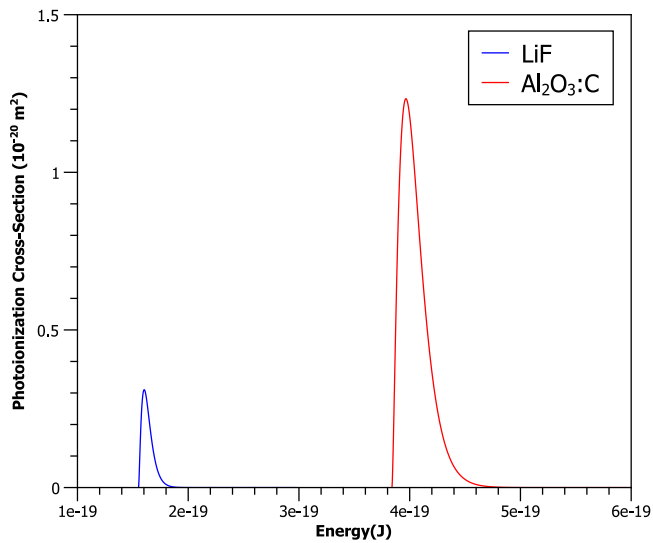


Fig. 5. Photoionization cross-section vs. electromagnetic radiation energy for two materials: LiF and  $\text{Al}_2\text{O}_3\text{:C}$ .

The maximum peak of the  $\text{Al}_2\text{O}_3\text{:C}$  presents one  $\sigma$  about 4 times greater than LiF.

It is possible to see that the peak maximum from  $\sigma$  of the  $\text{Al}_2\text{O}_3\text{:C}$  coincides with the frequency of the electromagnetic radiation in the blue range. The predictions of the present work agree well with the experimental data, in which the maximum emission of the OSL signal occurs in the blue stimulus for this material [39].

The magnitude of  $\sigma$  was also predicted to the specific wavelength,  $\lambda=470$  nm, the same wavelength used to stimulate the samples. In this case, the magnitude of  $\sigma$  for the  $\text{Al}_2\text{O}_3\text{:C}$  is much greater than for LiF:  $8.4 \times 10^{-21} \text{ m}^2$  and  $6.9 \times 10^{-50} \text{ m}^2$ , respectively. In fact, this difference is displayed in the OSL emission signal from both materials, as shown in Fig. 2a. In addition, it is also possible to see that LiF samples were submitted to 10 Gy and 15 Gy of absorbed dose, while  $\text{Al}_2\text{O}_3\text{:C}$  samples were submitted to 170 mGy. LiF was submitted to a much larger dose because it was not possible to see clearly the emission signal for lower doses. In general, as the dose deposited in the material increases, the number of electrons in trapping centers increases, and the intensity of the OSL emission signal is improved, showing its connection with the absorbed dose. It was not possible to irradiate both materials with the same dose because, to higher doses, the OSL signal of  $\text{Al}_2\text{O}_3\text{:C}$  could damage the photomultiplier, with no use of additional filtration. This makes a more accurate comparison difficult.

In order to analyze the pattern of OSL decays of both materials through the predictions of  $\sigma$ , the OSL intensity curve was plotted as a function of time by using the first-order kinetic model (Eq. (3)). The stimulated photon flux  $\phi$  with wavelength  $\lambda$  is the same for both materials. As the dose deposited in both samples are significantly different, the maximum value of  $\sigma$  ( $\sigma$  of the  $\text{Al}_2\text{O}_3\text{:C}$  is 4 times greater than LiF) has been considered with the goal of showing the entire tendency of the OSL decay pattern. Fig. 6 shows the normalized theoretical OSL curve based on Eq. (3). The theoretical predictions are very similar to the experimental results presented in Fig. 2b. The strong over-response of the initial intensity of the CW-OSL from  $\text{Al}_2\text{O}_3\text{:C}$  dosimeter is not shown in Fig. 6, because it is being considered the first-order kinetic (no retrapping) approximation in Eq. (3). This shows that the photoionization cross-section plays an important role in understanding the OSL decay curve. In addition, the results show that just linear effects are enough to describe the luminescent properties of these detectors.

Some points deserve special comments for the low OSL signal of LiF samples:

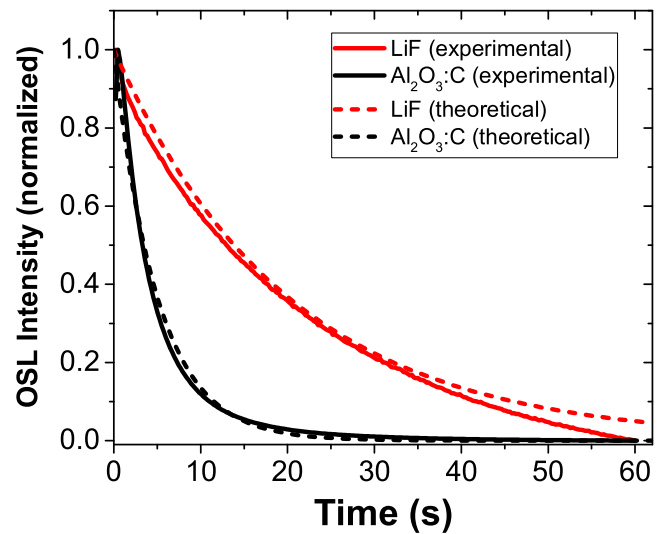


Fig. 6. Normalized OSL curves for the  $\text{Al}_2\text{O}_3\text{:C}$  and LiF samples. In this case, the maximum  $\sigma$  has been used in both materials. The solid line represents the normalized OSL experimental curves for  $\text{Al}_2\text{O}_3\text{:C}$  and LiF samples, irradiated with 170 mGy and 15 Gy respectively.

- The magnitude of the electron effective mass in this material is about 10 times greater than in the  $\text{Al}_2\text{O}_3\text{:C}$ . The magnitude of  $m^*$  influences the mobility of the electrons in the crystal lattice. As shown in the Ref. [19],  $\sigma$  increases with the decrease of  $m^*$ ;

- Although the phonon frequency is less in fluoride crystals, and in this case,  $\omega_0$  is about 2.5 times smaller than the  $\text{Al}_2\text{O}_3\text{:C}$ , it is not enough for causing major changes in the  $\sigma$ ;

- Thermoluminescence measures have shown shallow traps close to the edge of the conduction band (about 1 eV for LiF) [32]. Shallow traps are generally associated with the phosphorescence phenomena, which occur immediately after the irradiation. As the energy used to stimulate this material is about 2.6 times greater than the activation energy, the probability of transition is very low, according to the Fermi's golden rule. This makes the  $\sigma$  very low for the LiF;

- The magnitude of  $\sigma$  is maximum to  $\lambda=1240$  nm, because the activation energy of the trapping center corresponds to this wavelength;

- The low OSL signal of the LiF, even being irradiated with a high dose, is due to the photoionization cross-section that is very low. Both the intensity and the pattern of the OSL curve decay are governed by  $\sigma$  (see Eq. (3)). This behavior is shown in Figs. 2 and 6, in which the OSL curve slowly decays as well as the intensity is low.

The theoretical approach in this work based on the photoionization cross-section of the trapping center combined with the experimental data explains the main reasons for the low OSL signal emitted from LiF. For this,  $\text{Al}_2\text{O}_3\text{:C}$ , a commercial dosimeter, was used for comparison. From these results, it is possible to list some future perspectives to improve the OSL signal from this material.

One of them is to analyze the effect of dopants in this compound, because it may create traps or move them to deeper positions relative to the edge of the conduction band. Another mechanism is to analyze the behavior of the magnitude of the electron effective mass as well as the phonon frequency with the doping concentration.

## 5. Conclusions

In summary, in this work the photoionization cross-section ( $\sigma$ ) of trapped charge carriers in the trapping center was predicted for both compounds, LiF and  $\text{Al}_2\text{O}_3\text{:C}$ . For the same wavelength ( $\lambda=470$  nm) used to stimulate the samples, the magnitude of  $\sigma$  for the  $\text{Al}_2\text{O}_3\text{:C}$  is much greater than LiF:  $8.4 \times 10^{-21} \text{ m}^2$  and  $6.9 \times 10^{-50} \text{ m}^2$ , respectively. In addition, measurements of OSL show that even though the

absorbed dose is greatly lower in the case of  $\text{Al}_2\text{O}_3:\text{C}$  (submitted to 170 mGy), its OSL emission intensity is significantly higher than the one from LiF (submitted to 10 Gy and 15 Gy). For lower doses (in order of mGy), it was not possible to see the emission signal in LiF. The theoretical predictions of the OSL decay curve combine well with the experimental data. The combination of different methodologies shows that the low OSL signal of LiF is due to the very low magnitude of  $\sigma$  at the used excitation wavelength. Both the intensity and the pattern of the OSL curve decay are governed by  $\sigma$ . Finally, other factors as electron mobility and deep traps are crucial for improving the intensity of the OSL signal in this detector.

#### Declaration of competing interest

The authors declare that they have no known competing financial interests or personal relationships that could have appeared to influence the work reported in this paper.

#### CRediT authorship contribution statement

**Bruna Novais:** Conceptualization, Data curation. **Edward Ferraz:** Data curation, Writing - original draft. **Adelmo S. Souza:** Visualization, Investigation. **Patrícia L. Antonio:** Data curation, Formal analysis, Investigation, Methodology. **Linda V.E. Caldas:** Funding acquisition, Investigation, Methodology, Project administration. **João Batista:** Data curation, Formal analysis, Investigation, Methodology, Validation, Writing - original draft. **Heveson Lima:** Conceptualization, Formal analysis, Investigation, Project administration, Supervision, Validation, Visualization, Writing - original draft, Writing - review & editing.

#### Acknowledgments

The authors strongly acknowledge the financial support from Brazilian agencies CNPq (grant  $N_1$ . 301335/2016-8; grant  $N_2$ . 150117/2018-3, Post-doc fellowship of Patrícia L. Antonio), CAPES and FAPESB. The authors are also deeply grateful to Dr. Luiz C. Oliveira for valuable discussions.

#### References

- [1] T.T. Bushberg, J.A. Seibert, E.M. Leidholdt, J.M. Boone, *The Essential Physics of Medical Imaging*, Lippincott Williams & Wilkins, North America, 2011.
- [2] F.M. Khan, J.B. Gibbons, *The Physics of Radiation Therapy*, Lippincott Williams & Wilkins, North America, 2014.
- [3] M.R. Cleland, L.A. Parks, S. Cheng, *Nucl. Instrum. Methods Phys. Res. B* 208 (2003) 66–73.
- [4] E.G. Yukihara, S.W.S. McKeever, *Optically Stimulated Luminescence: Fundamentals and Applications*, John Wiley and Sons Ltd, Oklahoma, 2011.
- [5] R. Chen, V. Pagonis, *Thermally and Optically Stimulated Luminescence: A Simulation Approach*, Wiley, 2011.
- [6] R. Chen, S.W.S. McKeever, *Theory of Thermoluminescence and Related Phenomena*, World Scientific, 1997.
- [7] S.W.S. McKeever, M. Moscovitch, *Radiat. Prot. Dosim.* 104 (2003) 263–270.
- [8] L.C. Matsushima, G.R. Veneziani, L.L. Campos, *Radiat. Meas.* 56 (2013) 365–368.
- [9] Y. Lee, Y. Won, K. Kang, *Radiat. Prot. Dosim.* 164 (3) (2014) 1–7.
- [10] F. Tran, P. Blaha, *Phys. Rev. Lett.* 102 (2009) 22640.
- [11] H. Lima, M.A. Couto dos Santos, *J. Phys. Chem. Solids* 96–97 (2016) 38–41.
- [12] E.M. Yoshimura, E.G. Yukihara, *Nucl. Instrum. Methods Phys. Res. B* 250 (2006) 337–341.
- [13] L.C. Oliveira, E.G. Yukihara, O. Baffa, *Sci. Rep.* 6 (2016) 24348.
- [14] L. Oster, S. Druzhyina, Y.S. Horowitz, *Nucl. Instrum. Methods Phys. Res. A* 648 (2011) 261–265.
- [15] P. Bilski, B. Marczevska, A. Twardak, E. Mandowska, A. Mandowski, *Radiat. Meas.* 71 (2014) 61–64.
- [16] K.J. Kearfott, W.G. West, M. Rafique, *Appl. Radiat. Isot.* 99 (2015) 155–161.
- [17] E.G. Yukihara, S.W.S. McKeever, M.S. Akselrod, *Radiat. Meas.* 104 (2014) 15–24.
- [18] L. Botter-Jensen, S.W.S. McKeever, A.G. Wintle, *Optically Stimulated Luminescence Dosimetry*, Elsevier, Amsterdam, 2003.
- [19] H. Lima, J.V. Batista, M.A. Couto dos Santos, *Europhys. Lett.* 115 (2016) 33002.
- [20] E. Londero, E. Bourgeois, M. Nesladek, A. Gali, *Phys. Rev. B* 97 (2018) 241202(R).
- [21] J. Isberg, A. Tajani, D.J. Twitchen, *Phys. Rev. B* 73 (2006) 245207.
- [22] M. Şahin, *Phys. Rev. B* 77 (2008) 045317.
- [23] S.K. Panda, B. Pal, S. Mandal, M. Gorgoi, S. Das, I. Sarkar, W. Drube, W. Sun, I. Di Marco, A. Lindblad, P. Thunström, A. Delin, O. Karis, Y.O. Kvashnin, M. van Schilfhaarde, O. Eriksson, D.D. Sarma, *Phys. Rev. B* 93 (2016) 235138.
- [24] A.J.J. Bos, J. Wallinga, *Phys. Rev. B* 79 (2009) 195118.
- [25] L.C. Matsushima, G.R. Veneziani, R.K. Sakuraba, J.C. Cruz, L.L. Campos, *Appl. Radiat. Isotopes* 100 (2015) 7–10.
- [26] E.G. Yukihara, *Radiat. Meas.* 121 (2019) 103–108.
- [27] J.J. Sakurai, *Modern Quantum Mechanics*, Addison-Wesley, USA, 1994.
- [28] J.P. Perdew, K. Burke, M. Ernzerhof, *Phys. Rev. Lett.* 77 (1996) 3865–3868.
- [29] P. Giannozzi, S. Baroni, N. Bonini, M. Calandra, R. Car, C. Cavazzoni, D. Ceresoli, G.L. Chiarotti, M. Cococcioni, I. Dabo, A. Dal Corso, S. Fabris, G. Fratesi, S. de Gironcoli, R. Gebauer, U. Gerstmann, C. Gougousis, A. Kokalj, M. Lazzeri, L. Martin-Samos, N. Marzari, F. Mauri, R. Mazzarello, S. Paolini, A. Pasquarello, L. Paulatto, C. Sbraccia, S. Scandolo, G. Sclauzero, A.P. Seitsonen, A. Smogunov, P. Umari, R.M. Wentzcovitch, *J. Phys.: Condens. Matter.* 21 (2009) 395502.
- [30] P. Giannozzi, et al., *J. Phys.: Condens. Matter.* 29 (2017) 465901.
- [31] V. Pagonis, G. Kitis, *Phys. Status Solidi b* 249 (2012) 1590–1601.
- [32] M.A. Vallejo, M.A. Sosa, M.L. Villalobos, J.C. Azorín, R. Navarro, E. Encarnación, L.A. Díaz, *J. Lum.* 182 (2017) 160–165.
- [33] V.H. Whintley, S.W.S. McKeever, *J. Appl. Phys.* 90 (2001) 6073–6083.
- [34] E.G. Yukihara, V.H. Whintley, S.W. McKeever, A.E. Akselrod, M.S. Akselrod, *Radiat. Meas.* 38 (2004) 317–330.
- [35] C.R. Gopikrishnan, D. Jose, A. Datta, *AIP Adv.* 2 (2012) 012131.
- [36] M. Lisiansky, A. Heiman, M. Kovler, Y. Rosin, *J. Appl. Phys. Lett.* 89 (2006) 153506.
- [37] B.J. Ingram, T.O. Mason, R. Asahi, K.T. Park, A.J. Freeman, *Phys. Rev. B* 64 (2001) 155114.
- [38] M. Prencipe, A. Zupan, R. Dovesi, E. Aprà, V.R. Saunders, *Phys. Rev. B* 51 (6) (1995) 3391–3396.
- [39] N.K. Umisedo, E.M. Yoshimura, P.B.R. Gasparian, E.G. Yukihara, *Radiat. Meas.* 45 (2010) 151–156.